Development of a Novel Bio-Inspired Planetary Subsurface Explorer: Initial Experimental Study by Prototype Excavator With Propulsion and Excavation Units

Hayato Omori, *Member, IEEE*, Taro Murakami, Hiroaki Nagai, Taro Nakamura, *Member, IEEE*, and Takashi Kubota, *Member, IEEE*

***Abstract*—We have developed a novel planetary subsurface explorer that is capable of excavating lunar soil and carrying out scientific investigations. Our developed device consists of two units: a propulsion unit and an excavation unit. The propulsion unit that is based on the peristaltic crawling of earthworm maintains the body position and orientation of the robot and also reduces friction, which is the factor that traditionally prevents robots from excavating to significant depths. The excavation unit excavates and clears a space for the robot to tunnel into densely packed soil. In this paper, we discuss strategies for underground excavation. Next, we develop the excavation and propulsion units, and conduct several experiments to test these units. Finally, we develop a prototype subsurface robot with both units integrated in one package. The prototype exhibits good excavation performance in terms of depth reached—430 mm—both under its own full weight and for 1/6 of its own weight. In other words, the prototype shows excellent robustness to the gravity differences on the Earth and the Moon. With appropriate dust removal, operation has been demonstrated to a depth of 650 mm without any slowing down. The same performance is considered possible for much greater depths.**

***Index Terms*—Biomechanics, mobile robots, moon, space exploration.**

I. Introduction

PLANETARY exploration has great potential. It can lead to new discoveries, such as new substances, or help find keys to the origin of our planet [1]. Planetary investigations have provided basic information about the planets, such as geological, magnetic, and gravitational properties. However, many territories remain unexplored, particularly underground. Thus, scientific progress should be made in this area. However, some types of explorers launched from Planet Earth may take a long time to reach another planet. Small unmanned explorers will therefore be needed first, both for safety and economic reasons.

The Moon is the best-explored astronomical object so far. Many explorers and robots have been placed on its surface. In the Apollo program, astronauts took samples of regolith to a depth of around 3 m [2]. All this remains very limited though. We have therefore developed a small underground explorer that would be suitable for carrying out such important tasks on a larger scale.

A. Tasks for Lunar Explorer

Two typical tasks that an explorer is required to perform are the following: *in situ* scientific investigations or collecting samples at various depths; and installing devices for long-term investigations [3]. The former task will explain the formation of regolith and the effect of space environment such as solar storms and cosmic radiation as a function of soil depth. It is useful to be able to return to the surface on the Moon. A small number of robots could carry out investigations in different places and over vast areas of the lunar surface. In addition, *in situ* scientific devices could be installed to collect data and characteristics of less damaged material samples under harsh conditions in the space environment. More data and characteristics can be found using sample return devices after the collected samples are brought back to the Earth for further scientific investigations.

A seismometer is one of the required devices to detect crustal activity for the latter task. It should be placed at a target location of at least 1000 mm in depth. Moreover, a seismometer needs to be implanted in stable contact with its surroundings to measure minute quakes.

B. Previous Research

JAXA planned to use two penetrators in its Lunar-A project [4]. The similar penetrator is proposed in MoonLITE project [5]. The penetrators, which contained seismometers and heat-flow probes, would be loaded on a spacecraft. However, the proposed system did not have any mechanism to adjust for the attitude and depth of the penetrators after impact, and they would have largely disturbed the original conditions of the surroundings at

Manuscript received November 13, 2011; revised May 9, 2012; accepted September 16, 2012. Date of publication November 15, 2012; date of current version January 10, 2013. Recommended by Technical Editor A. Menciassi. This work was supported in part by Chuo University and in part by the Japan Aerospace Exploration Agency.

H. Omori and T. Nakamura are with the Department of Precision Mechanics, Chuo University, Tokyo 112-8551, Japan (e-mail: h_omori@bio.mech.chuo-u.ac.jp; nakamura@mech.chuo-u.ac.jp).

T. Murakami was with the Department of Precision Mechanics, Chuo University, Tokyo 112-8551, Japan. He is now with Rail Systems Company, Hitachi, Ltd., Ibaraki 317-8506, Japan.

H. Nagai was with the Department of Precision Mechanics, Chuo University, Kanagawa 237-8555, Japan. He is now with the Department of Robotics Application, Sumitomo Heavy Industries, Ltd., Tokyo 141-6025, Japan.

T. Kubota is with the Japan Aerospace Exploration Agency, Sagamihara 252-5210, Japan (e-mail: kubota@isas.jaxa.jp).

Color versions of one or more of the figures in this paper are available online at http://ieeexplore.ieee.org.

Digital Object Identifier 10.1109/TMECH.2012.2222429

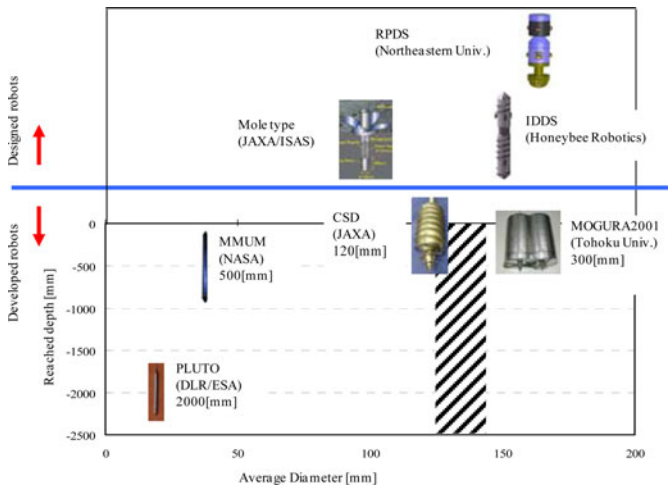

Fig. 1. Depth reached by various robots [7].

impact time. A micropenetrator [6], which is a type of explorer, consists of a drill and sampler subsystem. This system is expected to drill a small hole having diameter 1–2 m, deep into the surface, using low power and would be equipped with several scientific devices. However, as it drills deeper, the buckling problem in the drill becomes severe.

Fig. 1 shows the depth reached by various robots that have been developed, as well as those that have just been designed [7]. The part above the middle line shows robots that have been designed but have not yet been demonstrated in any excavation tests, whereas the part below the line shows the depths reached in excavation experiments by developed robots. The designed robots are plotted along the abscissa by the average diameter and the developed robots are plotted by average diameter against depth reached.

A detailed design for the robotic planetary drilling system included a propulsion unit, drill bit, and cuttings bucket [8]. It was designed according to typical, recommended specifications in terms of energy requirements [9] and was capable of moving along a curved path. However, this system has not yet been demonstrated. The inchworm deep drilling system was designed to drill deep into soil, ice, and rocks, mainly for exploring Mars and Europa [10]. It is expected to excavate to a depth of 0.001–1 km because of its lack of tether or umbilical cord, although no data of any actual excavation depths have been presented. One of the smallest excavators is the planetary underground tool (PLUTO), which uses a spring-loaded hammer [11] having a diameter of 20 mm, a length of 280 mm, and a mass of 0.35 kg. These features enable it to successfully excavate to a depth of around 2000 mm in simulated Martian soil. However, it does not have much space for scientific devices, except for a sampling device at the top. The Moon Mars underground mole (MMUM) [12] was based on a spring-loaded hammer similar to the one used in PLUTO. It is about twice as a large in size as PLUTO and has a mass of 2 kg. MMUM could reach a depth of around 500 mm in gritty dry sand. Two mole-type robots have also been developed. MOGURA2001 [13] consists of an excavating unit in front and a soil removal unit inside the robot. The excavation ability depends on the pushing force, which corresponds to its weight, because it does not have a supporting unit for propulsion. It could reach a depth of around 300 mm. The other mole robot was proposed by Kubota *et al*. [14]. They discussed a method for excavating, and demonstrated a robot's ability to carry and discharge soil using a test model, although no excavation data from their robot were reported. A robotic screw explorer [15], which has simple mechanism, is completely covered with screws. Front and rear screws rotate in opposite directions, which prevents the robot from rotating. The screw propulsion force is also used as a propulsion force for the robot. It could excavate 120 mm into fly ash, but stopped because of a structural issue.

By considering these previous robot designs, it can be inferred that as the excavator becomes larger, it is more difficult to excavate deep into the soil. We have developed an excavator having a size sufficient to carry a seismometer and *in situ* scientific investigation devices. Our developed excavator design will appear within the hatched area in Fig. 1. The earth pressure acting on the outer surface of an excavator increases as the excavator excavates deep. Then, the friction around it increases and prevents it from tunneling deep [13]. Hence, we have developed a subsurface explorer robot that features both propulsion and excavation units. The propulsion unit is based on the peristaltic crawling of earthworm and excavation unit is based on an earth auger (EA). Peristaltic crawling motion provides stability because the contracted body maintains contact with a large area of the surroundings, while the extending body from contracted is prevented from contact. The excavator is expected to decrease the blocking force for propelling deeper while maintaining the body position and orientation so that the excavation unit is not rotated. This arrangement should be able to excavate to deep depths.

In this paper, we first illustrate the features of peristaltic crawling in detail, and suggest a novel type of subsurface excavation method based on an earthworm. Next, an excavation unit using an EA and a propulsion unit using peristaltic crawling are individually developed, and are tested in several experiments. Then, we develop a prototype of the excavator improving as necessary both units and integrating them. This prototype proves capable to successfully excavate soil in experiments, and is even able to excavate deeper than the excavation unit alone, and than other existing developed excavators that have a similar diameter. In addition, it could excavate at the same depth, considering either gravity on Earth, i.e., coping with its own full weight and for 1/6 only of its own weight, i.e., typically for the conditions of the Moon.

In the end, it could excavate to a depth of 650 mm while getting rid of the excavated soil using a dust collector. These results thus showed that an excavator consisting two complementary units constitutes an appropriate mechanism for subsurface excavation.

II. Peristaltic Crawling of an Actual Earthworm

A. Mechanism of the Peristaltic Crawling

As a propulsion mechanism, an actual earthworm moves by peristaltic crawling [16], [17]. Fig. 2 shows the locomotion pattern of an earthworm during peristaltic crawling. First, the

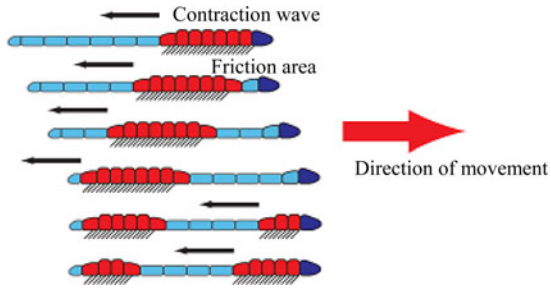

Fig. 2. Pattern of earthworm locomotion with peristaltic crawling.

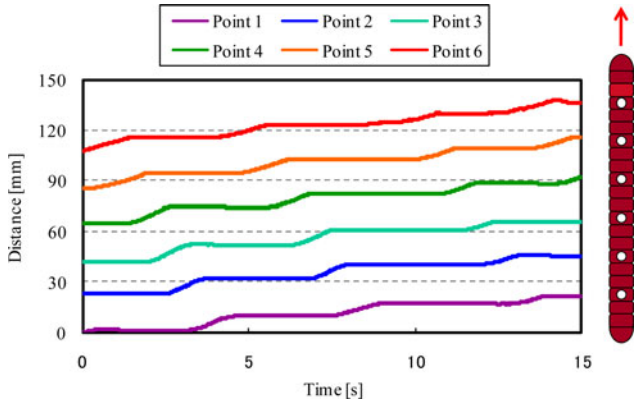

Fig. 3. Peristaltic crawling motion of the actual earthworm.

earthworm contracts its anterior segments. This increases the friction between the segments and the surrounding surface, as the thicker segments are in contact with the surface during locomotion. This friction generates a reaction force to extend the front contracted segments in the desired direction. The contraction propagates continuously toward the rear. This movement pulls the rear segments in the direction of movement. After the contraction is completed, the anterior segments of the earthworm are extended in the axial direction. There, each segment gets thicker in contracted mode, and thinner in extended mode during motion. This kind of locomotion is suitable for moving in perforated soil and is expected to provide stability in the underground, because the contracted body maintains contact with a large area of the surrounding soil, while the extended body is prevented from having contact to walls. This mechanism is therefore suitable for subsurface explorers.

B. Measurement of an Actual Earthworm's Peristaltic Crawling

We have observed a real earthworm, naturally expert at underground mining, and transposed its behavior on the robot. A 140–150-mm-long and 4–6-mm-thick earthworm was used. Markers were placed on the earthworm's segments every 19–25 mm (see Fig. 3). The locomotion was videotaped with a digital video camera and analyzed using a motion analysis software (MOVIAS Pro: Nac Image Technology Inc., Tokyo, Japan). The results obtained are shown in Fig. 3. This figure shows that the anterior part moves forward, then the posterior part moves forward along with the anterior part. Therefore, the contraction begins from the anterior part of the earthworm and continuously

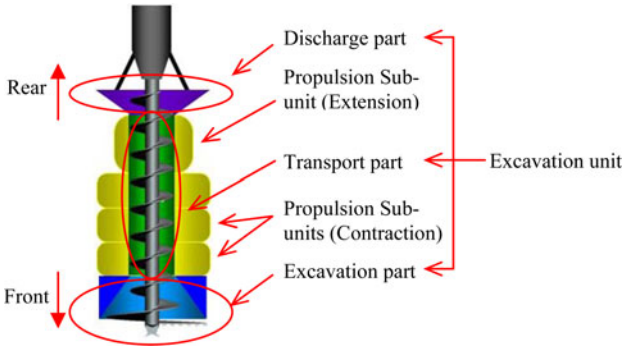

Fig. 4. Concept of the proposed underground explorer.

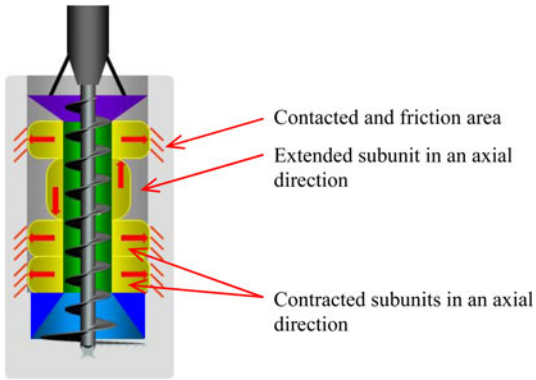

Fig. 5. Functioning of propulsion subunits inside a hole.

propagates toward the posterior part. The anterior segments contract again after propagation to the posterior part is complete. The average velocity of the earthworm was 16.1 mm/s. The peristaltic crawling robot was designed by taking these results into consideration.

III. Novel Subsurface Explorer Robot

In this section, we explain the concept of our underground explorer robot. The robot consists of two elements: a propulsion unit and an excavation unit (see Fig. 4). We adopted the peristaltic crawling behavior of an earthworm as the motion principle for the propulsion unit, and chose an EA as an excavation tool. The propulsion unit of the robot consists of four subunits corresponding to the individual segments of an earthworm. Fig. 5 shows their functioning while performing a peristaltic motion. Each subunit can contract and extend in the axial direction, and expand in the radial direction while contracting in the axial direction, thereby ensuring a high degree of friction between the body of the robot and its surroundings. Conversely, units that are extended in the axial direction do not make contact with their surroundings. The excavation unit of our prototype robot includes an EA with three parts allowing the following specific duties: excavation, transport, and discharge. The EA digs the hole, the front part excavates the material, and the screw part transports the excavated material to the rear of the EA. The robot excavates underground by making full use of these mechanisms. Fig. 6 details the motions involved in implementing the excavation process.

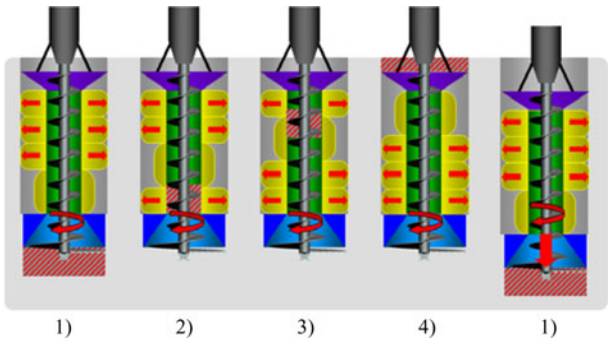

Fig. 6. Motions of excavation involved in excavation process.

1) Each contracted subunit maintains contact with the wall of the hole, maintaining its body position and orientation, thereby coping with the perturbations induced by the rotating action of the excavating EA. At the same time, the EA excavates material in front of the robot.

2-4) Extension propagates toward the rear, and the spiral of the EA (the transport component) carries excavated material to the rear of the unit, where it is discharged.

4-1) The second and third subunits from the front contract and sustain their positions. The front subunit extends to the front because the second and third subunits sustain their positions, and the extension force is applied in a downward direction, while the rear subunit contracts, permitting the robot to effectively move downward.

The excavation robot repeats Phases 1–4 to excavate its way underground. The front unit contracts in the radial direction, and thus does not generate friction with the wall of the hole, when the robot moves downward as a result of performing Phase 4–1. Thus, the robot decreases the effect of friction that traditionally limits propulsion. The same amount of material is discharged at the rear end of the robot as is excavated from its front end; however, the volume of excavated material is much larger than that of the packed material in front of the robot. The robot takes full advantage of the propulsion unit, which is able to move not only downward but also upward, by using the peristaltic crawling motion of the propulsion unit. In upward movement, the robot contracts from the rear subunit and propagates itself to the front subunit. By doing so, the robot can climb back to the surface level and discharge excavated material onto the surface of the ground. It then climbs back down to the bottom of the excavated hole. This feature also enables the robot to proceed to other areas to conduct more experiments once it has completed a scientific investigation in one area.

IV. Development of an Excavation Unit

We have developed an excavation unit to be later combined with the propulsion unit. Several excavation experiments were carried out with the excavation unit alone to examine the effect of friction with the walls of the hole, to estimate possible excavation depth, and to obtain realistic requirements for the propulsion unit.

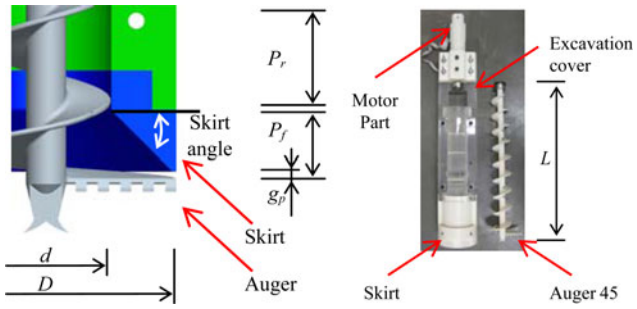

Fig. 7. EA for the propulsion unit.

TABLE I
Specifications of the Excavation Unit

D [mm]	130	Skirt angle [deg]	45
d [mm]	65	L [mm]	425
P_f [mm]	20	g_p [mm]	7.3
P_r [mm]	55	Total mass [kg]	5.9

A. Development of Tapering EA

The excavation part of the proposed robot excavates a hole with the same diameter as the propulsion unit, thus allowing the robot to advance. In addition, the excavated soil is carried through the propulsion unit by the turning of the EA. Therefore, the diameter of the EA must narrow down between the excavation part and the transport part. We have developed an auger that tapers in diameter by using the fishtail single-spiral type [18]–[20]. Fig. 7 and Table I show the characteristics and specifications of the excavation unit. The front pitch P_f is shorter than P_r to decrease the amount of excavated soil that gets stuck because of the narrowing of the auger. Since peristaltic crawling requires at least three rings (subunits), we consider it useful for this robot to have four units, thus providing enough force. Then the robot is able to move with several propulsion patterns, and it can sustain its position with at most two contracted units. The EA is 538 mm long, which is longer than the combined four units used for peristaltic crawling taking into account a length of discharge part. A DC motor (Maxon EC-Max) controls the rotation of the EA (see Fig. 7). Inside, excavation covers are used to cover the transport part. The excavation cover also combines the skirt with the motor cover so that the skirt does not move under the influence of the EA and the excavated soil. In the end, the PVC plate covers the outside of excavation cover to flatten out any possible irregularities.

B. Excavation Experiment Setup

Fig. 8 shows the excavation experimental setup. It is composed of the excavation unit, flames, linear guides, the wire sensor, counterweights, and reddish soil. The rear end of the motor part is fixed on the linear guides with a plate. The rotation of the excavation unit is reduced, and the excavation unit is able to excavate downward smoothly due to the linear guides. The counterweight is also fixed to the rear end of the motor part through a wire. The force pushing into the excavated soil is controllable at the beginning of the excavation experiments by

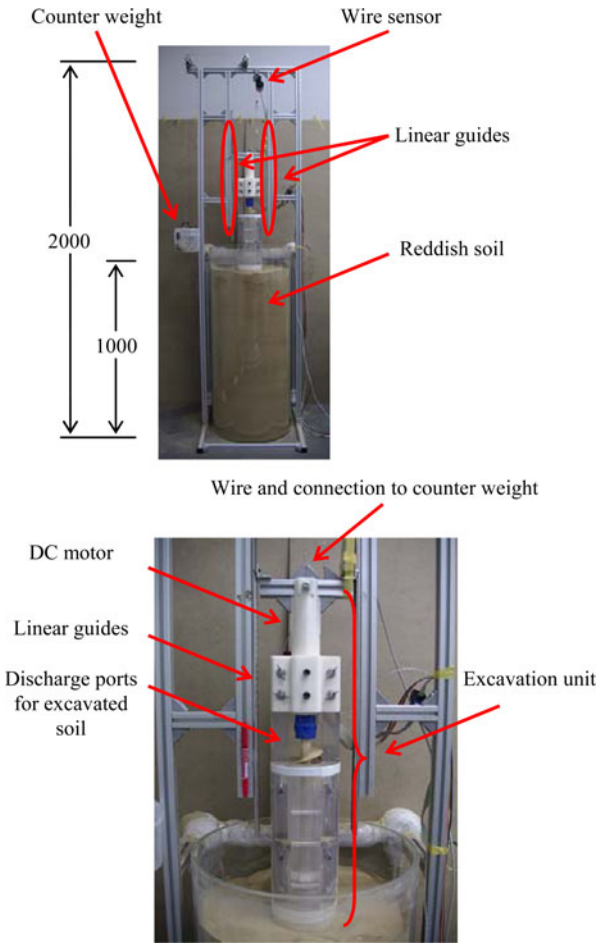

Fig. 8. Experimental setup.

TABLE II
SOIL CHARACTERISTICS [25]

	Bulk density [g/cm^3]	Internal friction angle [deg]
Regolith	1.45~1.79	42
Regolith simulant	1.4~2.0	37.2
Reddish soil	1.1~1.4	34.6

changing the counterweights. In the experiments, we measure the depth of excavation and motor torque while EA is excavating the reddish soil. The wire sensor measures the depth of excavation. We obtain motor torque by the output current from the motor driver. Table II compares the internal friction angles between regolith and regolith simulant [21].

C. Excavation Experiments

As stated, the excavation unit is a separate unit and does not have a propulsion mechanism. While this unit is excavating, the friction from the surrounding environment increases and prevents the unit from excavating further. Thus, the excavation unit is not able to generate sufficient pushing force to continue digging. The depth of excavation is clearly related to the weight of the unit. To clarify this relationship, we conducted two types of excavation experiments. In the first experiment, we changed the pushing force, whereas in the second experiment, we changed the speed of rotation. In the pushing-force experiments, we measured excavation depth and motor torque as functions of the pushing force. It is expected that the larger the pushing force is, the deeper the unit can dig because of the friction around the unit. The motor torque was also examined when the pushing force was the same as expected to be applied by the propulsion unit, in order to best prepare combinations of the excavation and propulsion units (see Section V). In the rotation-speed experiments, the unit was expected to show that the excavation velocity changes when the rotation speed is increased. The depth of excavation should remain constant at any velocity because the pushing force is the same.

Fig. 9. Experimental results of developed EA.

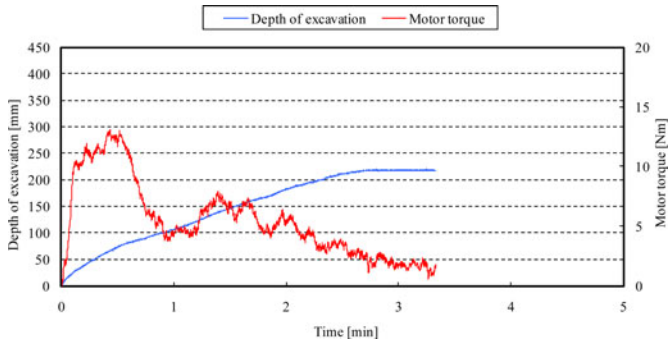

Fig. 10. Tracks of excavation (10 r/min, 52 N).

1) Changing the Pushing Force: In this experiment, we changed the counterweights used to alter the pushing force, and measured the depth of excavation and the current intensity corresponding to the motor torque. At the beginning of the experiments, the pushing forces were 52 N (weight of the robot including both the propulsion and the excavation units as described in Section VI), 26 N (1/2 of 52 N), 13 N (1/4 of 52 N), 55 N (extension force of a subunit, see Section V), and the rotation speed was 10 r/min. Each experiment was conducted five times. Fig. 9 shows one of these experiments and the excavation unit excavating soil.

All the experiments were essentially similar in terms of functional result. Fig. 10 shows the depth of excavation and motor torque over elapsed time under the constraints of 10-r/min velocity and 52-N force. As seen, the excavation velocity was fast for the first 50 s and maintained at an almost constant average velocity until approximately 2.5 min, where it slowed to nearly zero shortly afterward. The robot excavated to a depth of 219 mm. The motor torque increased for about 50 s, then gradually decreased.

Fig. 11 shows the effect of changing the pushing forces in four steps. Each bar on the left depicts the average reached

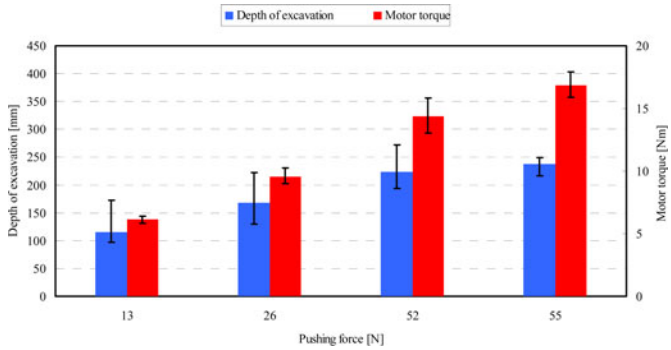

Fig. 11. Depth of excavation (left scale) and maximum motor torque (right scale) for different pushing forces (horizontal axis).

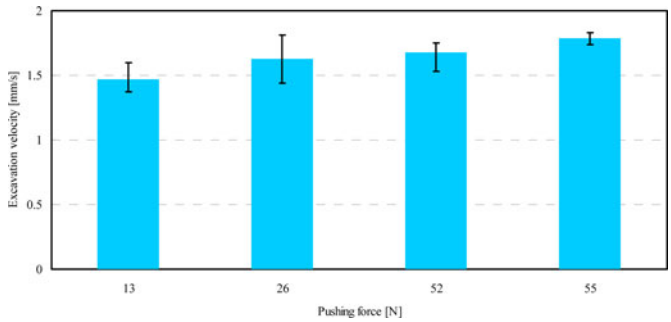

Fig. 12. Relationship between the pushing force and the excavation velocity.

depth of excavation of the five experiments and the bars on the right depict the average maximum excavation torque. Lines on the top of bars indicate the maximum and the minimum values. Fig. 12 shows the excavation velocity versus the pushing force. As seen in Fig. 11, the depth of excavation demonstrates a difference of about 100 mm between maximum and minimum, and the motor torque has a difference of about 3 N·m. These uncertainties are probably related to random variations in the soil. From these experimental results, we conclude that both the depth of excavation and the motor torque rise in value when the pushing force is large, whereas the velocity slightly increases when the pushing force is increased.

The maximum motor torque shows about 18 N·m at 55 N of the pushing force, and the propulsion unit needs to maintain the body position orientation against this torque.

2) Changing Rotation Speeds: In this experiment, we changed the rotation speed of EA and measured the depth of excavation and the motor torque. The pushing force was set to 52 N, and the rotation speeds were 3, 5, and 10 r/min.

We obtained experimental results similar to those shown in Fig. 10. Fig. 13 shows the depth of excavation and the motor torque as functions of auger rotary speed. The depths reached were almost the same in the three cases. The required motor torque shows slight differences with the rotation speed. The maximum motor torque was measured as 15.7 N·m at 3 r/min.

Fig. 14 shows the excavation velocity as proportional to the rotation of EA. The fastest velocity was 1.75 mm/s at 10 r/min. We realized that when the EA rotates fast, it can excavate fast even though it is required to generate almost the same motor torque as when rotation is slow.

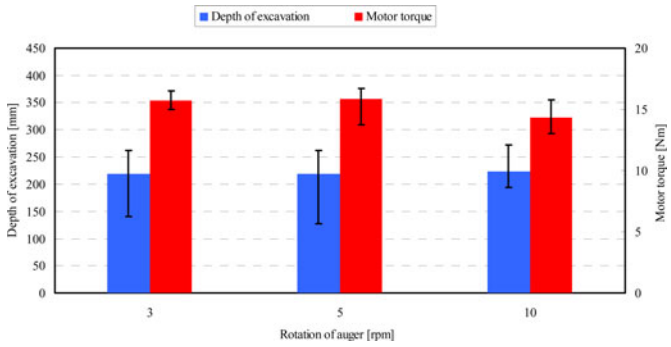

Fig. 13. Relationship between rotation speed and depth of excavation.

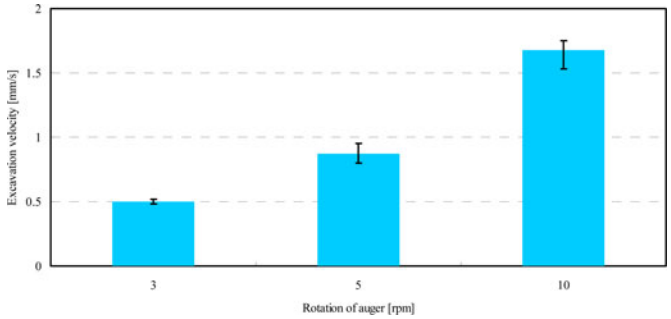

Fig. 14. Comparison of excavation velocities.

3) Conclusion of Experiments With Excavation Unit: Throughout these first experiments, the excavation unit as tested alone (i.e., without the propulsion unit as added in a later phase—see in the following) was able to excavate to quite a depth with a large weight. The unit can excavate to a similar depth, but faster, when the EA rotates faster. We confirmed that the friction caused by soil, piled up around the body of the unit, decreases the pushing force of this type of excavator, and limits its ability to excavate deeper. The reachable excavation depth totally depends upon the pushing force. Thus, one strategy to enable the unit to dig deeper is to increase the mass of the excavator. It is not possible, however, to rely on mass alone under gravity conditions such as those on the Moon. Thus, an additional mechanism is required to decrease the effect of the friction generated from the piled up soil. Therefore, we developed a propulsion unit that also maintains the orientation of the body position against a maximum rotation reaction force of around 18 N·m. This value would be decreased with propulsion units because the movement of a subunit can be controlled.

V. Development of a Propulsion Unit

A. Development of a Propulsion Subunit

A variety of earthworm robots have been developed using different actuators [22]–[27], with some motors being suitable for an explorer operating in a vacuum and for use in conditions where temperatures vary widely. Taking these developments into account, we developed an earthworm robot that uses servomotors and can move downward as well as upward in perforated soil [28]. Initially, this robot was neither equipped with an excavation tool for boring holes in the soil nor could generate

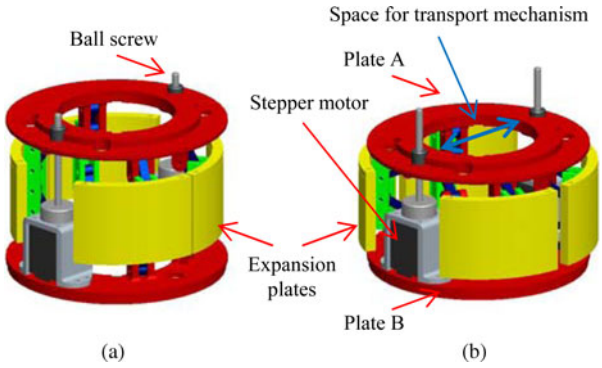

Fig. 15. Developed subunit, a ring actuated by dual pantographs. (a) Extension. (b) Contraction.

TABLE III
SPECIFICATIONS OF A UNIT

Max plate distance [mm]	84.0
Minimum plate distance [mm]	46.5
Max thickness [mm]	144
Minimum thickness [mm]	124
Diameter of space [mm]	65.0
Mass [kg]	0.51
Material	ABS

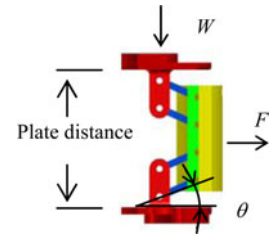

Fig. 16. Details of a dual pantograph.

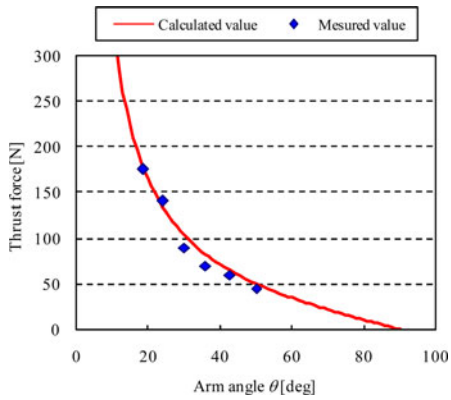

Fig. 17. Thrust force of a unit.

enough force to withstand the rotation action of the excavation unit.

A new propulsion unit was required to resist the maximum rotation action of the excavation unit and supply the appropriate weight to balance the vertical force of the robot mass, and therefore, we developed a propulsion element (a subunit or an actuated ring) corresponding to a single segment of a natural earthworm. Fig. 15 shows the structure of this device and Table III lists its specifications. The subunit has two stepper motors and ball screws to 1) generate contraction and extension forces that are large enough to withstand the rotary action of the excavation unit, and 2) move plate A with respect to parallel plate B to enable smooth contraction and extension movements. The stepper motors and ball screws control the contraction and extension of the actuated ring. As the subunit contracts, a dual pantograph extends in the radial direction. An expansion plate is attached to the dual pantograph, and this expansion plate also expands in the radial direction; thus, it can push in parallel against the surface of the walls of a hole. In addition, the expansion plate has a large circular arc area to maintain contact with the wall surface, which maintains body position during the rotation action of the EA. The subunit has two actuators and a large space of 65 mm in diameter, thus allowing for an additional transport mechanism to be located in the center of the unit.

The thrust force of the dual pantograph shown in Fig. 16 is given in (1), where the thrust force is F, the contraction force is W, and the arm angle is θ. From this equation, it can be seen that when the unit fully contracts, the thrust force is maximum

$$F = \frac{W}{\tan\theta}. \tag{1}$$

B. Experiments With Actuated Ring

We developed a prototype excavation robot that moves inside a launcher (a tube providing initial support and guidance) and digs a hole in a tube initially full of soil (the details of the excavation process are explained in Section VII-A and are shown in Fig. 20). In this section, we carry out experiments to test whether an actuated ring can resist the rotary action of the excavation unit and ensure the vertical reaction force necessary to balance the weight of the robot.

We first measured the extension and contraction forces of the unit and the thrust force that the unit exerts on the walls of the hole using a load cell. The extension force and contraction force in the radial direction corresponded to W in Fig. 16 and were measured as 55 N, almost the same, regardless of the plate distance. Thus, the thrust force was obtained. Fig. 17 shows the experimental results of the thrust force and the calculated values. These calculated values are obtained from (1) with W taken as 55 N, as measured previously. Thus, in practice, the actuated ring generates nearly the same thrust force as the calculated values. Such a unit generates a relatively large expansion force when it contracts.

Next, we measured the rotation action and the vertical support force of the unit. Experiments were conducted inside a launcher 131 mm in diameter and in a dirt hole 130 mm in diameter. The reaction force resulting from the ring balances the rotation action of the EA. The vertical support force supports the weight and the propulsion force caused by the EA during excavation. In measuring the vertical support force, a unit was positioned in the contracted state inside the launcher and dirt hole, and the contracted unit's expansion plates are in contract with them. The unit was pulled with a spring balance. In the measurement of the rotation support force, a unit was set up under the same

TABLE IV
EXPERIMENTAL RESULTS IN A LAUNCHER AND SOIL

	Launcher	Soil
Rotation reaction [Nm]	7	4.8
Vertical support force [N]	100	32

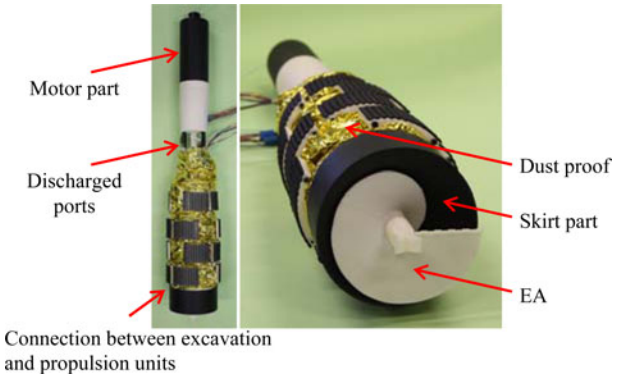

Fig. 18. Developed buried robot.

conditions as for measuring vertical support force, and turned. Table IV lists the experimental results. The vertical support force in the launcher was set to 100 N to maintain body position. This can be achieved with one contracted unit—balancing the robot weight and a pushing force of 55 N. The force in the soil was 32 N; therefore, at least two units are needed to maintain body position. The maximum rotation reaction capacity in a launcher was 7 N·m and that in soil was estimated as 4.8 N·m. The maximum rotation action force of the excavation unit was about 18 N·m in the experiments conducted with the excavation unit. As such, the device does not meet our requirements. However, possible improvements are as follows: different materials for expansion plates, surfaces with tiny projections, and increased area of the launcher could make it work properly, both inside the launcher and in the soil.

VI. DEVELOPMENT OF A SUBSURFACE EXPLORER

Both the excavation unit and the propulsion unit were developed separately in the first phase, and a series of experiments were conducted. In this section, we developed a prototype of a subsurface explorer, which improves upon the previous individual designs and integrates the two units.

A. Prototype Robot Integrating Propulsion and Excavation Units

Fig. 18 shows the developed robot. It consists of four propulsion rings, each of which has four expansion plates. Additional rubber friction sheets are placed on the outer surface of the expansion plates, which increase the friction forces while the robot is moving inside a launcher. These plates cover a large area of the outer surface of the unit. The remaining uncovered spaces, i.e., the gaps between the propulsion units and those between expansion plates, are covered with dustproof material (aluminium evaporation sheets) to prevent soil from getting inside the rings. These sheets are positioned so as not to hinder the contraction and extension of the unit. The excavation unit connects the front of the propulsion unit, and the transport part passes through, inside the propulsion rings. A DC motor located at the rear end of the robot powers the EA. The excavated soil is discharged from discharge ports behind the propulsion unit. The total mass of the prototype robot is 5.28 kg and its length is 800 mm.

B. Control System

We made this system as functional yet as simple as possible for the prototype robot. A design for use in an actual mission in space in terms of robustness of implementation is a possible future extension of the project. In the experiments, the excavation and propulsion units are controlled in a distributed way, each including their respective resources. For the excavation unit, a PC controls the DC motor via a motor driver. The motor rotates at a constant speed with the feedback data received from an encoder. The PC also monitors the current level, which is approximately proportional to the motor torque. In the propulsion units, an H8 microcontroller controls the stepper motors.

C. Propulsion Velocity

Altering the extension or contraction phases of each unit can achieve several motion patterns of the robot. Motion patterns consist of a wavelength, propagation speed, and number of waves. Here, wavelength is defined as the number of units extended in the axial direction. The propagation speed is the number of subunits propagated in the rear. We identify the basic motion patterns as an *l–s–n* motion (wavelength–propagation speed–number of waves). The developed robot includes four subunits, and we use the pattern 1-1-1, which is depicted in the yellow propulsion unit of Fig. 6.

The extension speed of a unit v is given as follows:

$$v = \frac{dP}{Pt}. \tag{2}$$

Here, the top plate of a subunit moves a d (μm) distance when a pulse signal is sent to stepper motors. P is the number of pulse signals from the H8 microcontroller. The time t (μs) is the cycle length of a pulse signal.

Then, propulsion speed V (mm/s) is given as follows:

$$V = v\frac{l}{N} = \frac{dl}{Nt}. \tag{3}$$

Here, N is the total number of subunits, 4 for this robot. The robot moves with a 1-1-1 pattern and moves forward by the difference of contraction and extension of one subunit. l is multiplied to v because it is the number of subunits simultaneously extended. v is divided by N because the robot moves forward once in a cycle of N motions.

D. Propulsion Experiments in a Pipe

We compare the downward propulsion velocity V in (3) with its experimented equivalent in a pipe. The 1-1-1 propulsion pattern was used for this experiment. Marks were placed in the middle of each unit and analyzed using a motion analysis software. Target velocities were set at 0.5 and 1.0 mm/s values.

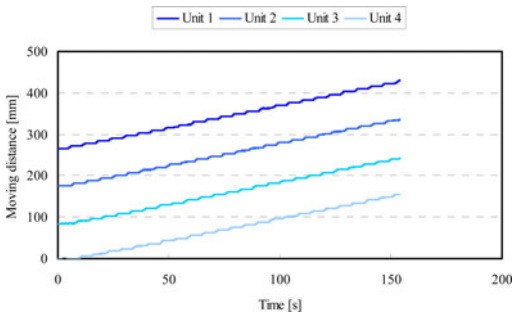

Fig. 19. Movement tracks of the propulsion unit.

TABLE V
VELOCITY COMPARISONS

Desired velocity [mm/s]	Theoretical velocity [mm/s]	Experimental velocity [mm/s]
0.50	0.50	0.47
1.00	1.00	1.06

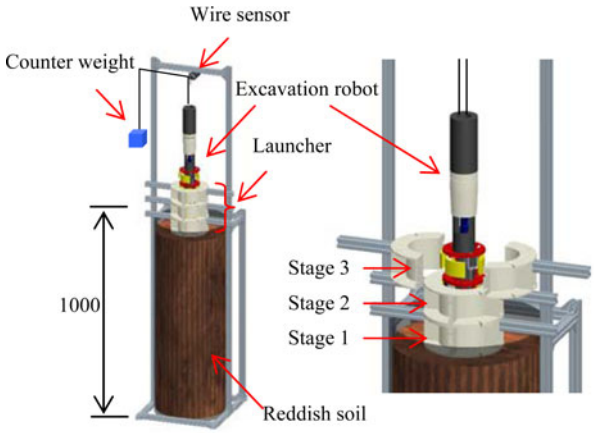

Fig. 20 Experimental setup.

The tracks of marks are shown in Fig. 19 for a speed of 1.0 mm/s. The front subunit first contracts, then this contraction propagates to the rear subunit in the same fashion as a natural, living earth worm does in Fig. 3. Table V shows experimental and calculated velocities. Slight differences are visible; nevertheless, we can conclude that the robot moves as planned.

VII. EXCAVATION EXPERIMENTS

A. Experimental Setup

Fig. 20 shows the experimental excavation setup for the developed robot. It consists of the robot, a wire sensor, a launcher, counterweights, and reddish soil. The launcher, which supports peristaltic crawling until the robot reaches the soil, would be installed on a rover in an actual mission. The launcher is made of ABS and has three stages, covering three rings of the propulsion unit from the front. The robot is able to move using peristaltic crawling, but needs at least three units to generate this kind of locomotion. Each stage can be separated to avoid covering the discharge ports of the robot. In this experiment, the rotation speed of the EA was set at 10 r/min. A 1-1-1 propulsion pattern was used, and the ring extension velocity was set at 1.0 mm/s. The robot velocity is 0.25 mm/s as validated in an earlier section. Here, we measure the depth of excavation and motor torque. The wire sensor measures the depth of excavation. We obtain the level of motor torque from the current output of the motor driver. The experiments continued until the discharge ports reached soil level.

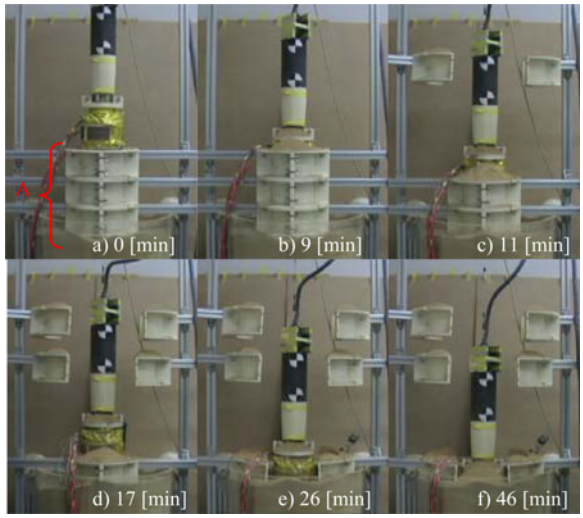

Fig. 21. Excavation experiments with launcher (A: Launcher).

For possible future missions, the excavator could operate on the Moon or other bodies with a gravity six times less intense than that of the Earth. The developed device has been tested for excavation experiments in similar, lighter weight conditions by using counterweights. The forces applied to the EA were set at 1/1, 1/2 (26 N), 1/4 (13 N), and 1/6 (8.7 N) of its own weight on Earth of 52 N.

B. Experimental Results for Various Excavation Conditions

Fig. 21 shows the experimental process. This process can be described in six phases, as given in the following.

1) Beginning of the experiment.
2) Discharge ports reaching Stage 3.
3) Stage 3 of the launcher separated to both sides.
4) After Stage 2 separation.
5) After Stage 1 separation.
6) Excavation stopped when discharged ports reached soil level.

Fig. 22 shows the experimental results in terms of depth of excavation and motor torque as functions of time. As shown in this figure, the excavation velocity mainly changed at approximately 9 min when the robot was released from the top stage of the launcher. Then, for 1 or 2 min, the velocity became faster than that prior to this 9-min mark. The motor torque also increased because of this slip. At this point, the front ring was moving in the soil and the other rings were moving in the launcher. We assume that it was difficult to generate enough friction force because the surface of shallow soil was weak and not packed. Excavation remained constant until the bottom stage of the launcher was released. From this point on, the robot continued excavating although the velocity decreased. We investigated the hole and the robot after excavation. It seemed that the

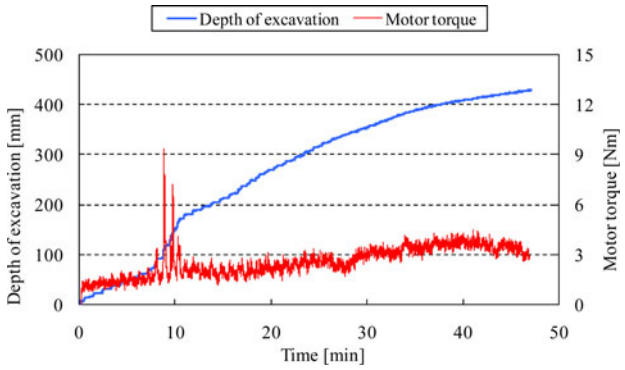

Fig. 22. Results of excavation.

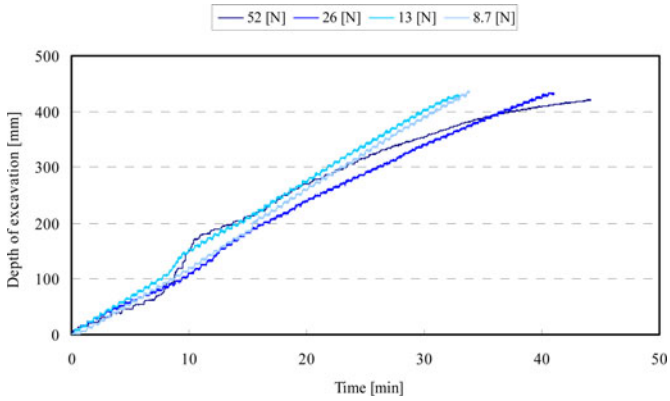

Fig. 23 Experimental results of different weights of the excavator.

discharged soil then fell into the hole, preventing the propulsion unit from working properly. The experimental results for the excavation unit alone appear to be almost straight in Fig. 10. In contrast, the results for the new robot, with both units integrated, clearly depict a stair shape in Fig. 22, and the robot did not just fall down through the hole under its own weight, but succeeded in moving using peristaltic crawling. The robot could excavate to a depth of 430 mm, i.e., deeper than the excavation unit alone. The maximum torque was kept to less than 10 N·m, which was about 40% less than that of the excavating unit alone and favorable for overall robot motion. Except for a few seconds at this relatively large motor torque, throughout about 1-h experiment, motor torque could be further reduced by more than 70% (see Fig. 22).

Fig. 23 shows the experimental results, in terms of depth with respect to elapsed time, for the four excavation conditions used in the experiment. The average velocity of excavation was 0.19 mm/s at 52 N, 0.19 mm/s at 26 N, 0.23 mm/s at 13 N, and 0.21 mm/s at 8.7 N. The average velocities, for cases in which the experimental mass was 1/4 and 1/6 of the robot's weight, were similar to the target velocity of 0.25 mm/s. But the velocities at 1/2 and 1/1 of the robot's weight were lower. We believe this occurred because discharged soil fell into the excavated hole and prevented the propulsion unit from working properly. However, the excavator could bore to a depth of around 430 mm, and was expected to be able to excavate deeper because the excavation velocity did not decline except when progressing under its own

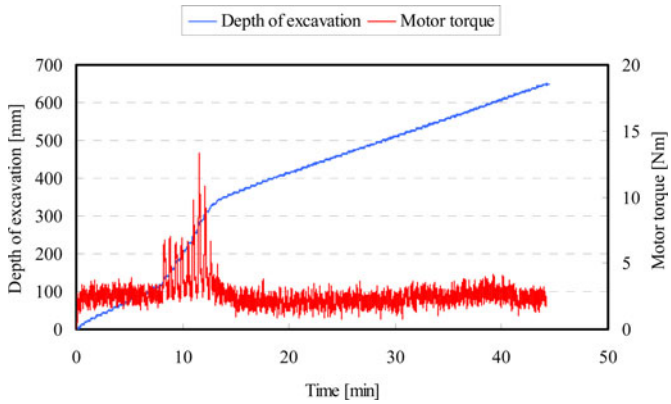

Fig. 24. Results of excavation with the dust collector.

full weight. Slippage was also observed as the motor torque increased, but the average motor torque was reduced to less than 5 N·m.

Through experiments, we confirmed that the excavator was able to excavate and move at 1/6 of its own weight. Excavation deeper than 430 mm is possible by improving the discharge part of the unit. Therefore, we concluded that the propulsion unit can maintain its body position and rotation for the most part, therefore reducing the effect of the pressure of the surrounding earth in terms of controlling "wall holding" during downward movement.

Both the developed propulsion and excavation units proved effective for use in the prototype excavation robot.

C. *Experiments With Dust Collector*

As presented in previous section, the robot was able to excavate to a depth of 430 mm, then it had to stop excavating because the discharged ports reached soil level. Then, it seemed impossible to discharge further the excavated soil.

Here, we report on the excavation experiments after a depth of the discharged ports reached soil level, now getting rid of the excavated soil using a dust collector. Fig. 24 shows the tracks of measured excavation depth and motor torque. The robot moved inside the launcher for the first 9 min, at an average velocity of 0.23 mm/s. Then it "slipped" from 9 to 13 min in a transition phase, while the launcher was being released. Then, it constantly excavated from 13 min to the end of experiments. Here, the average velocity was 0.16 mm/s. It could excavate to a depth of 650 mm until a hose pipe was unable to reach (see Fig. 25). In this experiment, the dust collector omitted the soil from the discharged ports. The robot could excavate to a depth of 650 mm, the tracks of excavation was constant, and the velocity did not get slower. We believe that it could easily excavate deeper than 650 mm, if the discharging process were improved. The proposed propulsion unit has demonstrated that it decreases the effect of the friction force traditionally limiting excavator locomotion. Therefore, we confirm that the bioinspired propulsion unit relying on peristaltic crawling and the principle of a taper EA work greatly for an excavation robot.

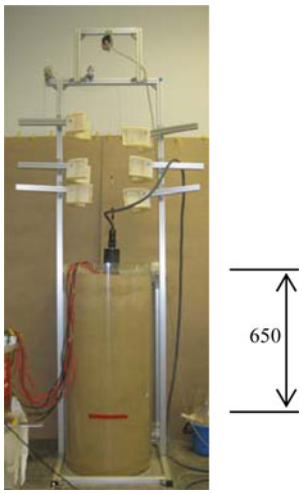

Fig. 25. Robot excavating a depth of 650 mm.

D. Additional Considerations—Energy and Mechatronics

The mechatronic approach adopted for this project allowed the integration of several simple yet robust technologies to yield a smart result. The most evident aspect of this strategy was the distributed nature of resources where drilling, tool progress, and energy sources can be individually optimized, and then coordinated using sensors and control components. Even at a subunit scale, e.g., for propulsion, the bioinspired peristaltic approach is similar in strategy, relying ultimately on the passive friction forces of virtually unlimited intensity, at a power requirement practically as low as desired. The proposed system can comply with typical recommended specifications in terms of energy requirements [9] and classical energy sources can easily be considered and put to use in our design. As tested previously, the robot can be powered by electrical cables, requiring a consumption of about 40 W, supplied by batteries, solar panels, or nuclear sources, which can be left in location on the surface. Other recent examples of mechatronic approaches to similar topics can be found in other literature [29]–[32].

VIII. Conclusion

We observed a real earthworm, naturally expert at underground mining, and transposed its behavior to a machine-based artifact, developing a prototype of a subsurface robot with two main components: one for propulsion and one for excavation. The excavator begins excavation from inside a launcher that would be loaded on a rover on an actual mission. This paper has progressively introduced all the successful elements, improving at each stage upon the success of earlier phases. The excavation unit working alone was able to successfully excavate a hole, and experiments were conducted to a depth of 219 mm under gravity alone. The propulsion unit also proved capable of driving the excavating unit. In particular, the unit was able to reduce 1) motor torque requirements by supporting it; and 2) the risk of the motor stalling by transferring the ripped material all the way through the excavator, from the front to rear of the device. Experiments were conducted to a depth of 430 mm regardless of planetary gravity. Finally, the excavator was tested with the addition of a dust collector that gets rid of excavated soil from the discharge ports. Our experiments showed that such an excavator can reach a depth of 650 mm without slowing down at a speed of about 0.16 mm/s for an average motor torque of about 2.5 N·m. We believe that it is possible to excavate deeper. In light of these findings, we can confirm that an excavator using both proposed units would be suitable for a subsurface explorer.

The excavator could be improved in a future project by adapting it so that it exclusively consists materials designed for cosmic environments. The outer surface of the expansion plates could be improved and friction-rich features such as spike projections could be considered for this improvement. We are also developing a discharge-assistance mechanism to enable the robot to excavate deeper than its own length. Likewise, the control system can also be improved, integrating better excavation and propulsion tasks and implementing them on a single PC-typed resource, including all sensor feedback. In addition, as future tasks, excavation experiments should be carried out using many different types of soil such as regolith and Martian simulant. The climbing up and down experiments would also be tested.

Acknowledgment

The authors would like to thank Prof. Dessimoz from HEIG-VD for the help and advice. They would also like to thank the anonymous reviewers who made many valuable comments, which improved this paper.

References

[1] R. Mattingly and L. May, "Mars sample return as a campaign," in *Proc. IEEE Aerosp. Conf.*, Big Sky, MT, Mar. 2011, pp. 1–13.
[2] O. G. Morris, "Apollo 17 Mission report," Lyndon B. Johnson Space Center, NASA, Houston, TX , Rep. JSC–07904, Mar. 1973.
[3] S. Nishida and S. Wakabayashi, "A plan for lunar exploration by using robots," in *Proc. Int. Symp. Artif. Intell., Robot. Autom. Space*, Sapporo, Japan, 2010, pp. 594–599.
[4] H. Shiraishi, S. Tanaka, A. Fujimura, and H. Hayakawa, "The present status of the Japanese penetrator mission: LUNAR-A," *Adv. Space Res.*, vol. 42, no. 2, pp. 386–393, Jul. 2008.
[5] Y. Gao, A. Phipps, M. Taylor, I. A. Crawford, A. J. Ball, L. Wilson, D. Parker, M. Sweeting, A. D. S. Curiel, P. Davies, A. Baker, W. T. Pike, A. Smith, and R. Gowen, "Lunar science with affordable small spacecraft technologies: MoonLITE and Moonraker," *Planet. Space Sci.*, vol. 56, pp. 368–377, 2008.
[6] Y. Gao, A. Ellery, M. Jaddou, J. Vincent, and S. Eckersley, "Planetary micro-penetrator concept study with biomimetric drill and sampler design," *IEEE Trans. Aerosp. Electron. Syst.*, vol. 43, no. 3, pp. 875–885, Jul. 2007.
[7] K. Nagaoka, T. Kubota, M. Otsuki, and S. Tanaka, "Experimental analysis of a screw drilling mechanism for lunar robotic subsurface exploration," *Adv. Robot.*, vol. 24, nos. 8–9, pp. 1127–1147, 2010.
[8] Y. Liu and B. Weinberg, "Mechanical design and modelling of a robotic planetary drilling system," in *Proc. ASME Int. Des. Eng. Tech. Conf. Comput. Inform. Eng. Conf.*, Philadelphia, PA, 2006, pp. 925–932.
[9] H. Rabia, "Specific energy as a criterion for drill performance prediction," *Int. J. Rock Mech. Mining Sci. Geomech. Abstr.*, vol. 19, pp. 39–42, 1982.
[10] S. P. Gorevan, T. M. Myrick, C. Batting, S. Mukherjee, P. Bartlett, and J. Wilson, "Strategies for future mars exploration: An infrastructure for the near and longer-term future exploration of the subsurface of mars," presented at the 6th Int. Conf. Mars, Pasadena, CA, 2003.
[11] L. Richter, P. Coste, V. V. Gromov, H. Kochan, R. Nadalini, T. C. Ng, S. Pinna, H.-E. Richter, and K. L. Yung, "Development and testing of subsurface sampling devices for the Beagle 2 lander," *Planet. Space Sci*, vol. 50, pp. 903–913, Aug. 2002.
[12] C. R. Stoker, A. Gonzales, and J. R. Zavaleta, "Moon/mars underground mole," presented at the NASA Sci. Technol. Conf., Adelphi, MD, 2007.

[13] K. Yoshida, N. Mizuno, T. Yokoyama, H. Kanamori, M. Sonoyama, and T. Watabe, "Development of a mole-type robot for lunar/ planetary subsurface exploration, and its performance evaluation," presented at the 20th Annu. Conf. Robot. Soc. Jpn., Osaka, Japan, 2002, Paper 1J35.
[14] T. Kubota, K. Nagaoka, S. Tanaka, and T. Nakamura, "Earthworm typed drilling robot for subsurface planetary exploration," in *Proc. IEEE Int. Conf. Robot. Biomimetics*, Sanya, China, Dec. 2007, pp. 1394–1399.
[15] K. Nagaoka, T. Kubota, M. Otsuki, and S. Tanaka, "Robotic screw explorer for lunar subsurface investigation: Dynamics modelling and experimental validation," in *Proc. Int. Conf. Adv. Robot.*, Munich, Germany, 2009, pp. 1–6.
[16] H. Sugi, *Evolution of Muscle Motion*. Tokyo, Japan: Univ. Tokyo Press, 1977, p. 72.
[17] R. M. Alexander, *Exploring Biomechanics: Animals in Motion*. San Francisco, CA: Freeman, 1992.
[18] H. Omori, T. Nakamura, T. Yada, T. Murakami, H. Nagai, and T. Kubota, "Excavation mechanism for a planetary underground explorer robot," in *Proc. Int. Symp. Robot.*, Munich, Germany, 2010, pp. 1273–1279.
[19] H. Omori, T. Nakamura, T. Murakami, H. Nagai, and T. Kubota, "An earth auger as excavation part for a planetary underground explorer robot using peristaltic crawling," in *Proc. Int. Symp. Artif. Intell., Robot. Autom. Space*, Sapporo, Japan, 2010, pp. 784–789.
[20] A. Kato, "Excavating machines and particular kind of excavation," *Jpn. Soc. Civil Eng.*, pp. 73–78, 1979.
[21] S. Wakabayashi and K. Matsumoto "Development of slope mobility tested using simulated lunar soil," Japan Aerospace Exploration Agency Res. Dev. Memorandum, Sagamihara, Japan, 2006.
[22] M. Takahashi, I. Hayashi, N. Iwatsuki, K. Suzumori, and N. Ohki, "The development of an in-pipe microrobot applying the motion of an earthworm," *Jpn. Soc. Precis. Eng.*, vol. 61, no. 1, pp. 90–94, 1995.
[23] A. Menciassi, S. Gorini, G. Pernorio, and P. Dario, "A SMA actuated artificial earthworm," in *Proc. Int. Congr. Robot. Autom.*, New Orleans, LA, 2004, pp. 3282–3287.
[24] N. Saga and T. Nakamura, "Development of a peristaltic crawling robot using magnetic fluid on the basis of the locomotion mechanism of the earthworm," *Smart Mater. Struct.*, vol. 13, pp. 566–569, 2004.
[25] N. Saga and T. Nakamura, "A prototype of peristaltic robot using pneumatic artificial muscle," *Intell. Autom. Syst.*, vol. 8, pp. 85–95, 2004.
[26] J. Zuo, G. Yan, and Z. Gao, "A micro creeping robot for colonoscopy based on the earthworm," *J. Med. Eng. Technol.*, vol. 29, pp. 1–7, 2005.
[27] A. S. Boxerbaum, H. J. Chiel, and R. D. Quinn, "A new theory and methods for creating peristaltic motion in a robotic platform," in *Proc. Int. Conf. Robot. Autom.*, Anchorage, AK, 2010, pp. 1221–1227.
[28] H. Omori, T. Nakamura, and T. Yada, "An underground explorer robot based on peristaltic crawling of earthworms," *Ind. Robot.: Int. J.*, vol. 36, no. 4, pp. 358–364, 2009.
[29] P. Liljeback, K. Y. Pettersen, O. Stavdahl, and J. T. Gravdahl, "Snake robot locomotion in environments with obstacles," *IEEE Trans. Mechatronics*, vol. 17, no. 6, pp. 1158–1169, Dec. 2012.
[30] J. Morales, J. L. Martinez, A. Mandow, J. Seron, and A. J. Garcia-Cerezo, "Static tip-over stability analysis for a robotic vehicle with a single-axle trailer on slopes based on altered supporting polygons," *IEEE Trans. Mechatronics*, [Online]. Available: http://ieeexplore.ieee.org, 10.1109/TMECH.2011.2181955.
[31] J. Qiao, J. Shang, A. Goldenberg, and A. Goldenberg, "Development of inchworm in-pipe robot based on self-locking mechanism," *IEEE Trans. Mechatronics*, [Online]. Available: http://ieeexplore.ieee.org, 10.1109/TMECH.2012.2184294.
[32] K. Ning and F. Worgotter, "Control system development for a novel wire-driven hyper-redundant chain robot, 3D-trunk," *IEEE Trans. Mechatronics*, vol. 17, no. 5, pp. 949–959, Oct. 2012.

Hayato Omori (M'10) was born in Kanagawa, Japan, in 1985. He received the B.S.E. and M.S.E. degrees in precision mechanics from Chuo University, Tokyo, Japan, in 2008 and 2010, respectively, where he is currently working toward the doctoral degree in precision mechanics.

His research interests include biomechatronics, robotics, and excavating technologies.

Mr. Omori is a member of the Robotics Society of Japan and the Japan Society of Mechanical Engineers. He received the Industrial Robot Innovation Award Highly Commended Award at the International Conference on Climbing and Walking Robots in 2008.

Taro Murakami was born in Nagano, Japan, in 1985. He received the B.S.E. and M.S.E. degrees in precision mechanics from Chuo University, Tokyo, Japan, in 2009 and 2011, respectively.

He is currently with the Rail Systems Company, Hitachi, Ltd., Ibaraki, Japan. His research interests include biomechatronics, robotics, and mechatronics.

Hiroaki Nagai was born in Nagano, Japan, in 1987. He received the B.S.E. and M.S.E. degrees in precision mechanics from Chuo University, Tokyo, Japan, in 2010 and 2012, respectively.

He is currently with the Robotics Application Department, Sumitomo Heavy Industries, Ltd., Kanagawa, Japan. His research interests include biomechatronics, robotics, and mechatronics.

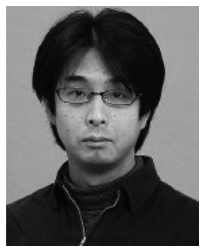

Taro Nakamura (M'04) was born in Saitama, Japan, in 1975. He received the Ph.D. degree from Shinshu University, Nagano, Japan.

From 1999 to 2004, he was an Assistant Professor at Akita Prefectural University. In 2004, he became a Lecturer in the Faculty of Science and Engineering, Chuo University, Tokyo, Japan, where he became an Associate Professor in 2006. He was a visiting Professor at the Ecole Polytechnique Fédérale de Laussane, Switzerland, from 2012 to 2013. His research interests include applications of smart material devices, biomechatronics, and robotics.

Dr. Nakamura received the Industrial Robot Innovation Award Highly Commended Award at the International Conference on Climbing and Walking Robots in 2008, the 2009 Young Investigation Excellence Award from the Robotics Society of Japan (RSJ), the 2010 Japan Society of Mechanical Engineers (JSME) Young Engineers Award, and the Young Scientists' Prize for Science and Technology from the Minister of Education, Culture, Sports, Science and Technology. He is a member of the RSJ and JSME.

Takashi Kubota (M'86) was born in Urawa City, Japan, in 1960. He received the B.E. degree in electronic engineering and the M.E. and Ph.D. degrees in electrical engineering from The University of Tokyo, Tokyo, Japan, in 1986, 1988, and 1991, respectively.

From 1991 to 1993, he was involved in the Myway Project at Fujitsu Laboratories Ltd. In 1993, he joined the Institute of Space and Astronautical Science (ISAS), Japan, where he was an Associate Professor. He was a Visiting Scientist in Jet Propulsion Laboratory in 1997 and 1998. He is currently a Professor at the ISAS, Japan Aerospace Exploration Agency, Sagamihara, Japan. He is also a Professor in the Graduate School of The University of Tokyo. He is a Co-Chair of the Space Education and Awareness Working Group, Asia-Pacific Regional Space Agency Forum. He was in charge of guidance, navigation, and control of the asteroid exploration mission HAYABUSA. His research interests include artificial intelligence in space, robotics, and image-based navigation.

Dr. Kubota is a member of the Robotics Society of Japan and the Society of Instrument and Control Engineers of Japan.